Dynamics of Atom-Mediated Photon-Photon Scattering II: Experiment

M. W. Mitchell, Cindy I. Hancox and R. Y. Chiao
Department of Physics, University of California at Berkeley, Berkeley, CA 94720, USA
(February 8, 2001)

Temporal and angular correlations in atom-mediated photon-photon scattering are measured. Good agreement is found with the theory presented in Part I.

I. INTRODUCTION

As described in Part I [?], atom-mediated photon-photon scattering is the microscopic process underlying the optical Kerr nonlinearity in atomic media. The Kerr nonlinearity produces such effects as self-phase modulation, self-focusing and self-defocusing and four-wave mixing. In an atomic medium, resonanant nonlinearities can give rise to very large nonlinear optical effects, suggesting the possibility of nonlinear optical interactions with only a few photons [?]. Unfortunately, the same resonances which could facilitate such experiments make them difficult to analyze [?]. In Part I we showed theoretically that the photon-photon interaction is not intrinsically lossy, and can be fast on the time scale of atomic relaxation. Here we describe an experiment to directly measure the time-duration of the photon-photon interaction in a transparent medium.

In the scattering experiment, two off-resonance laser beams collide in a rubidium vapor cell and scattering products are detected at right angles. The process of phase-matched resonance fluorescence in this geometry has been described as spontaneous four-wave mixing [?], a description which applies to our off-resonant excitation as well. This geometry has been of interest in quantum optics for generating phase-conjugate reflection [?]. Elegant experiments with a barium atomic beam [?] showed antibunching in multi-atom resonance fluorescence, but a separation of timescales was not possible since the detuning, linewidth and doppler width were all of comparable magnitude.

II. SETUP

A free-running 30mW diode laser at 780nm was temperature stabilized and actively locked to the point of minimum fluorescence between the hyperfine-split resonances of the D2 line of rubidium. Saturation spectroscopy features could be observed using this laser, indicating a linewidth $\delta\nu < 200$ MHz. This linewidth is small compared with the detuning from the nearest absorption line $\delta\nu = 1.3$ GHz . Direct observation of the laser output with a fast photodiode (3 dB rolloff at 9 GHz) showed no significant modulation in the frequency band 100 MHz – 2 GHz. The laser beam was was shaped by passage through a single-mode polarization-maintaining fiber, collimated and passed through a scattering cell to a retro-reflection mirror. The beam within the cell was linearly polarized in the vertical direction. The beam waist (at the retroreflection mirror) was 0.026 cm $\times$0.023 cm (intensity FWHM, vertical $\times$ horizontal). The center of the cell was 1.9 cm from the retroreflection mirror, thus within a Rayleigh range of the waist. With optimal alignment, the laser could deliver 1.95 mW to the cell, giving a maximal Rabi frequency of $\Omega_{\mathrm{Rabi}} \approx 2 \times 10^9 \mathrm{s}^{-1}$, significantly less than the minimal detuning of $\delta = 2\pi \times 1.3$ GHz $= 8 \times 10^9 \mathrm{s}^{-1}$. For this reason, we have neglected saturation of the transitions in the analysis.

The retro-reflected beam returned through the fiber and was picked off by a beamsplitter. The single-mode fiber acted as a near-ideal spatial filter and the returned power through the fiber provides a quantitative measure of the mode fidelity on passing through the rubidium cell. With optimal alignment it was possible to achieve a mode fidelity (described below) of 36%.

The cell, an evacuated cuvette filled with natural abundance rubidium vapor, was maintained at a temperature of 330 K to produce a density of about 1.6 $\times 10^{10}$ cm^{-3}. Irises near the cell limited the field of view of the detectors. Stray light reaching the detectors was negligible, as were the detectors' dark count rates of < 100 cps.

With the aide of an auxiliary laser beam, two single-photon counting modules (SPCMs) were positioned to detect photons leaving the detection region in opposite directions. In particular, photons scattered at right-angles to the incident beams and in the direction perpendicular to the drive beam polarization were observed. Each detector had a 500 μm diameter active area and a quantum efficiency of about 70%. The detectors were at a distance of 70 cm from the center of the cell. The effective position of one detector could be scanned in two dimensions by displacing the alignment mirrors with inchworm motors. A time-to-amplitude converter and multichannel analyzer were used to record the time-delay spectrum. The system time response was measured using sub-picosecond pulses at 850nm as an impulse source. The response was well described by a Lorentzian of width 810 ps (FWHM).

Optimal alignment of the laser beam to the input fiber coupler could not always be maintained against thermal drifts in the laboratory. This affected the power of the

drive beams in the cell but not their alignment or beam shape. These were preserved by the mode-filtering of the fiber. Since the shape of the correlation function depends on beam shape and laser tuning but not on beam power, this reduction in drive power reduced the data rate but did not introduce errors into the correlation signal.

A. Experimental Results

The time-delay spectrum of a data run of 45 hours is shown in Fig. 2. The detectors were placed to collect back-to-back scattering products to maximize the photon-photon scattering signal. A Gaussian function $P(t_A - t_B)$ fitted to the data has a contrast $[P(0) - P(\infty)]/P(\infty)$ of 0.046 ± 0.008, a FWHM of 1.3 ± 0.3 ns, and a center of -0.07 ± 0.11 ns. This center position is consistent with zero, as one would expect by the symmetry of the scattering process. For comparison, a reference spectrum is shown. This was taken under the same conditions but with one detector intentonally misaligned by much more than the angular width of the scattering signal.

The angular dependence of the scattering signal was investigated by acquiring time-delay spectra as a function of detector position. To avoid drifts over the week-long acquision, the detector was scanned in a raster pattern, remaining on each point for 300 s before shifting to the next. Points were spaced at 1 mm intervals. Total live acquisition time was 9 hours per point. The aggregate time-spectrum from each location was fitted to a Gaussian function with fixed width and center determined from the data of Fig. 2. The position-dependent contrast C(x,y) is shown in Fig. 3. A negative value for the contrast means that the best fit had a coincidence dip rather than a coincidence peak at zero time. These negative values are not statistically significant. Fitted to a Gaussian function, C(x,y) has a peak of $0.044 \pm .010$ and angular widths (FWHM) of 1.1 ± 0.7 mrad and 3.7 ± 0.4 mrad in the horizontal and vertical directions, respectively.

These angular widths are consistent with the expected coherence of scattering products [**?**]. Seen from the detector positions, the excitation beam is narrow in the vertical direction, with a Gaussian shape of beam waist $w_y = 0.009$ cm, but is limited in the horizontal direction only by the apertures, of size $\Delta z = 0.08$ cm. Thus we expect angular widths of 0.9 mrad and 3.25 mrad, where the first describes diffraction of a Gaussian, the second diffraction from a hard aperture.

III. COMPARISON TO THEORY

The correlation signal predicted by the theory of Part I is shown in Fig. 4. The ideal contrast is 1.53 and the FWHM is 870 ps. The shape of the time correlations is altered by experimental limitations. First, beam distortion in passing through the cell windows reduces the photon-photon scattering signal. Second, finite detector response time and finite detector size act to disperse the signal. None of these effects alters the incoherent scattering background.

Beam distortion is quantified by the fidelity factor introduced in Part I

$$F \equiv 4 \frac{\left| \int d^3x G(\mathbf{x}) H(\mathbf{x}) \right|^2}{\left[\int d^3x \left(|G(\mathbf{x})|^2 + |H(\mathbf{x})|^2 \right) \right]^2} \tag{1}$$

The greatest contrast occurs when H is the phase-conjugate, or time-reverse of G, i.e., when $H(\mathbf{x}) = G^*(\mathbf{x})$. In this situation $F = 1$. Under the approximation that the field envelopes obey the paraxial wave equations

$$\begin{aligned} \frac{d}{dz} G &= \frac{i}{2k} \nabla_\perp^2 G \\ \frac{d}{dz} H &= \frac{-i}{2k} \nabla_\perp^2 H, \end{aligned} \tag{2}$$

Green's theorem can be used to show that the volume integral is proportional to the mode-overlap integral

$$\int d^3x G(\mathbf{x}) H(\mathbf{x}) = \Delta z \int dx dy G(\mathbf{x}) H(\mathbf{x}), \tag{3}$$

where the last integration is taken at any fixed z and Δz is the length of the interaction region. Similarly, the beam powers are invariant under propagation and the mode fidelity can be expressed entirely in terms of surface integrals as

$$\begin{aligned} F = 4 &\left| \int dx dy G(\mathbf{x}) H(\mathbf{x}) \right|^2 \\ &\times \left[\int dx dy \left(|G(\mathbf{x})|^2 + |H(\mathbf{x})|^2 \right) \right]^{-2}. \end{aligned} \tag{4}$$

The overlap of G and H also determines the efficiency of coupling back into the fiber. This allows us to determine F. In terms of $P_{\rm in}$, the power leaving the output fiber coupler and $P_{\rm ret}$, the power returned through the fiber after being retro-reflected, this is

$$F = \frac{4}{(1+T^2)^2} \frac{P_{\rm ret}}{\eta T P_{\rm in}}. \tag{5}$$

where $\eta = 0.883$ is the intensity transmission coefficient of the fiber and coupling lenses and $T = 0.92$ is the transmission coefficient for a single-pass through a cell window. We find $F = 0.36 \pm 0.03$. The mode fidelity acts twice to reduce contrast, once as the drive beams enter the cell, and again on the photons leaving the cell. This beam distortion has no effect on the incoherent scattering background, thus the visibility is reduced by F^2.

The finite time response of the detector system acts to disperse the coincidence signal over a larger time window. This reduces the maximum contrast by a factor of 0.27

and increases the temporal width to 1.62 ns. Similarly, the finite detector area reduces the maximum contrast by a factor of 0.81 and spreads the angular correlations by a small amount. The resulting coincidence signal is shown in Fig. 6. Fitted to a Gaussian, the final signal contrast is 0.042 $\pm$0.007, where the uncertainty reflects the uncertainty in F. This is consistent with the observed contrast of 0.044 $\pm$ 0.010.

IV. CONCLUSION

We have measured the temporal and angular correlations in photon-photon scattering mediated by atomic rubidium vapor. We found good agreement between experiment and the perturbative theory presented in Part I. The observed temporal correlations are of the order of one nanosecond, much faster than the system can relax by radiative processes. This is consistent with the prediction that the duration of the photon-photon interaction is determined by the inhomogeneous broadening of the vapor.

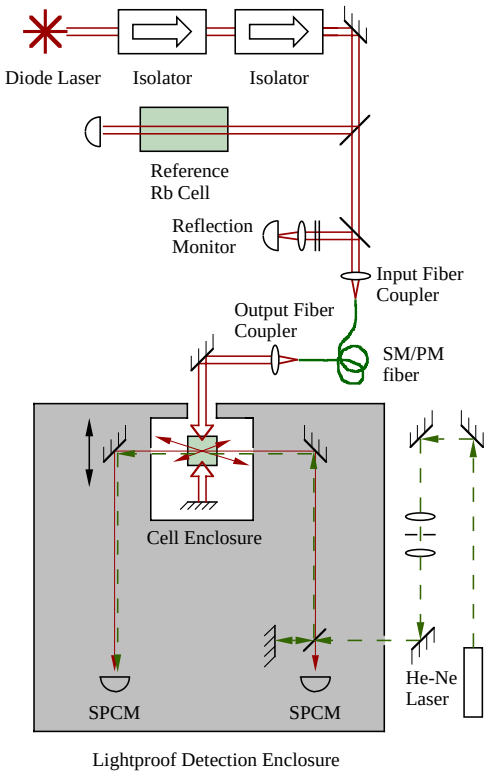

FIG. 1. FIG. 1. Experiment schematic.

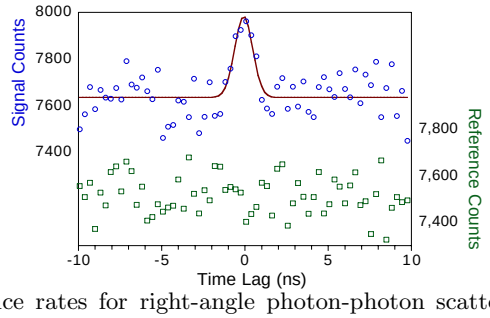

FIG. 2. FIG. 2. Observed coincidence rates for right-angle photon-photon scattering. Circles show data acquired with detectors aligned to collect back-to-back scattering products. Squares show data acquired with detectors misaligned by 10 cm $\approx$ 0.14 radian. The solid line is a Gaussian function fit to the data.

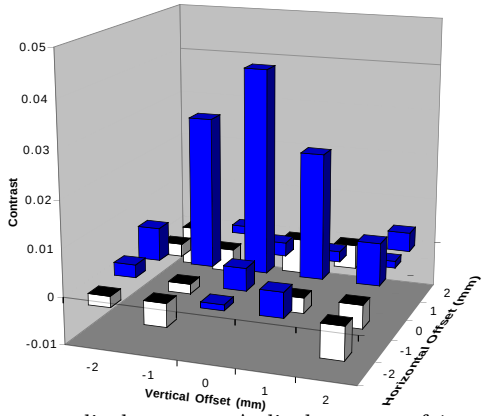

FIG. 3. FIG. 3. Signal contrast vs. detector displacement. A displacement of 1 mm corresponds to an angular deviation of 1.43 mrad.

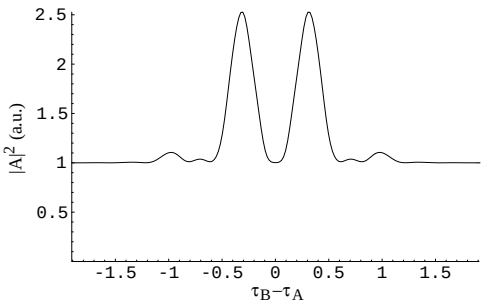

FIG. 4. FIG. 4. Coincidence rates by photon-photon scattering theory: ideal case.

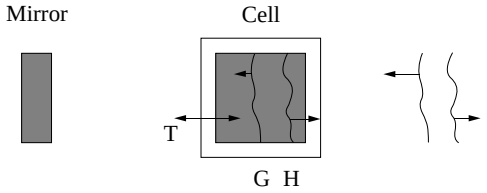

FIG. 5. FIG. 5. Geometry for retro-reflection measurements.

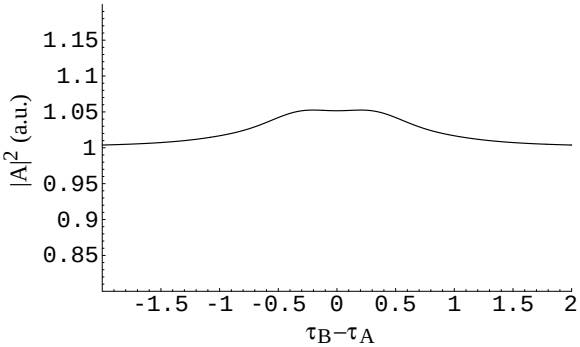

FIG. 6. FIG. 6. Coincidence rates by photon-photon scattering theory: adjusted for beam shape, finite detection time and detector area.